A Physical Model of Axonal Elongation: Force, Viscosity, and Adhesions Govern the Mode of Outgrowth

Matthew O'Toole,* Phillip Lamoureux,[†] and Kyle E. Miller[†]

*Department of Mathematics and [†]Department of Zoology, Michigan State University, East Lansing, Michigan

ABSTRACT   Whether the axonal framework is stationary or moves is a central debate in cell biology. To better understand this problem, we developed a mathematical model that incorporates force generation at the growth cone, the viscoelastic properties of the axon, and adhesions between the axon and substrate. Using force-calibrated needles to apply and measure forces at the growth cone, we used docked mitochondria as markers to monitor movement of the axonal framework. We found coherent axonal transport that decreased away from the growth cone. Based on the velocity profiles of movement and the force applied at the growth cone, and by varying the attachment of the axonal shaft to the coverslip, we estimate values for the axial viscosity of the axon ($3 \times 10^6 \pm 2.4 \times 10^6$ Pa·s) and the friction coefficient for laminin/polyornithine-based adhesions along the axon ($9.6 \times 10^3 \pm 7.5 \times 10^3$ Pa·s). Our model suggests that whether axons elongate by tip growth or stretching depends on the level of force generation at the growth cone, the viscosity of the axon, and the level of adhesions along the axon.

INTRODUCTION

Axonal elongation has been thought to occur through tip growth, where new material is added at the growth cone and the axonal framework is stationary (1–3). Although past studies suggest that axonal branch points and marks made along the axon remain stationary as the axon elongates (4–8), recent work suggests that in some cases there is a gradient of bulk transport of docked materials, with little or no transport seen in the proximal axon and increasing anterograde transport in the distal axon (9). This low-velocity transport (LVT) has been observed in the absence of growth-cone advance, which suggests that there is more to this than simple stretching of the axon. In addition, whether axons lengthen through tip growth or stretching in *Xenopus* neurons depends on whether they are grown on highly adhesive (concanavalin A) or permissive (laminin) substrates (10). These studies raise the questions of what role growth-cone-generated tension plays in elongation, and whether the mode of axonal elongation depends on the physical properties (adhesion to the substrate and viscosity) of the axon.

Mechanical tension has long been known to be an effective stimulus to axonal elongation/growth. Tension has been experimentally applied to lengthen existing neurites (11,12), and axons that are detached from their substrate not only stop elongating, but experience retraction (13). Mass addition to the neurite is another important aspect of axonal elongation that appears to be linked to tension. In one instance, elongation rates of 8 mm/day were achieved via mechanically applied tension (14). In that case, the neurons tended to increase in diameter (14) and were functionally normal (15). In another experiment, leg-lengthening procedures in adult rats caused doubling of the internodal distances, with no axonal thinning (16). These results indicate that the rate of mass addition to the axon increases in response to tension-induced lengthening. Further, the inability of microtubule-polymerizing drugs, such as taxol, to induce elongation (17) brings into question whether mass addition independently drives elongation. Mass addition is certainly an essential component of healthy axonal elongation, but the evidence suggests that tension at the growth cone is the factor that directly controls the rate of lengthening. Thus, we suggest that tension is the independent variable that determines the rate of axonal lengthening.

En bloc movement of the axonal cytoskeleton long went unnoticed as experimental observations focused on proximal regions of axons. Only when measurements were made in the distal axon was this phenomenon discovered. Photobleaching (10,18), photoactivation (19,20), and the tracking of docked mitochondria (9) have revealed that the cytoskeleton does move in an anterograde manner, but that this behavior diminishes with distance from the growth cone. That growth cones generate pulling forces and neurons grown in culture adhere to their substrates gives a possible insight to this observation. Any deformation of the axon as a result of growth-cone-generated tension will be most prominent in the distal region, but as that force is dissipated through adhesions, the effects will diminish. As the above experiments have shown, tension at the growth cone not only leads to lengthening, but may deform the distal region of the axon, resulting in en bloc movement of the cytoskeleton.

Deformations of materials can be elastic, where materials stretch like springs, or viscous, where materials flow as fluids (21). In this article, axonal stretching refers to both elastic and viscous deformation. It is important to note that whether axons behave mechanically as solids or fluids depends on the timescale of the observations. Rapid deformations over the

course of seconds to minutes lead to springlike behaviors. When axons are pulled slowly enough over the course of hours to days they can elongate viscously by many millimeters without breaking or thinning (14,15,22). The observation that lengthening occurs without a great degree of thinning suggests that mass addition to the axon is occurring. It is possible that when axons are stretched slowly mass addition can accommodate lengthening and lead to a physiological behavior that is primarily viscous.

Axonal elongation in response to force application at the growth cone (towing) has been described as occurring in three stages (22). After an initial elastic stretch, there is a period of delayed stretching, followed by elongation at a constant rate. This behavior has been modeled by Dennerll et al. (22) using a three-element model in which the axon behaved as a spring, a Voigt element, and a dashpot in series (Fig. 1 A). The combination is also known as a Burgers element (23). This model well describes the effects of tensile stress on the elongation of axons, but does not address deformation of the distal axon or the effects of adhesions along the axon.

Aeschlimann was the first to extend a general type of model to segments along the axon (24,25). In the Aes-

chlimann model, the axon is treated as a series of springs that elastically stretch, with a growth dashpot at the end of the axon where new mass is added. This accounted for the springlike behaviors axons exhibit over short time spans and the fluidlike behaviors associated with axonal lengthening. A further insight was the incorporation of viscous drag that was interpreted as being due to interactions between the axonal shaft and substrate. Although the Aeschlimann model is sophisticated in its integration of both the tip growth model and the biophysical properties of the axon, the following experimental data suggest to us that the axon is more accurately modeled as a series of dashpots that acts like a viscoelastic fluid: 1), Though rapid deformations over the course of seconds to minutes lead to springlike behaviors, when axons are pulled slowly enough over the course of hours to days they can elongate viscously by many millimeters without breaking or thinning (14,15,22). 2), Growth cones sometimes pause while the axon remains under tension. If axons behaved as viscoelastic solids, material along the axon would stop moving during a pause. In contrast, a viscoelastic fluid model predicts continued movement of the axonal framework toward the site of tension generation. Experiments have shown that bulk movement of material occurs during growth cone pauses (9). Thus, we suggest that the simplest model for the mechanical behavior of the axon is that of a viscoelastic fluid.

Here, we extend the Dennerll model to the entire axon; that is, we view each segment of the axon as consisting of a Burgers element. This allows us to study how tensile forces cause axonal stretching at each point along the length of the neurite in addition to elongation. By including the effects of extracellular adhesions along the length, we derive a model that captures both the effects of tension generation at the growth cone and dissipation along the length due to adhesions to the extracellular matrix substrates (10). We report that whether axons grow by stretching or by tip growth can be explained by varying the parameters in a single model that includes force, axonal mechanical behavior, and frictional interactions with the substrate.

MATERIALS AND METHODS

Cell culture

Chick sensory neurons were isolated as described by Sinclair et al. (26) from lumbosacral dorsal root ganglia of 11- to 12-day-old chicken embryos. Cells were grown at 37°C in L-15 medium (Sigma Chemical, St. Louis, MO) supplemented with 0.6% glucose, 300 mg/liter glutamine, 100 U/ml penicillin, 136 μM/ml streptomycin sulfate, 10% fetal calf serum, 50 ng/ml 7S nerve growth factor (Harlan Bioproducts, Indianapolis, IN), and N9 growth supplement. The culture surface was first treated with 0.01% polyornithine and rinsed. The surfaces were then treated with 20 ng/ml laminin.

Towing experiments

Mitochondria were labeled with 0.1 μM Mitotracker Red CMX-Ros (Molecular Probes, Eugene, OR) in L-15 medium for 2 min and then allowed
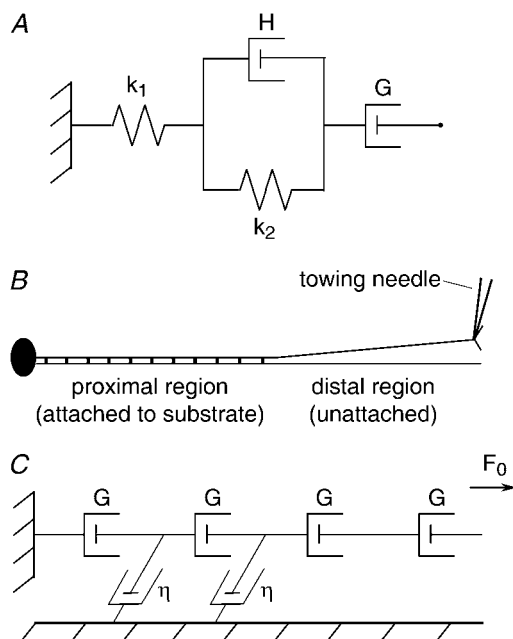

FIGURE 1   Model of a towed neurite as a series of dashpots. (A) We consider the axon as a series of Burgers elements. Each element consists of two elastic elements and a free dashpot (with constant G), which simulates towed growth. (B) Diagram of a neurite during towing. The distal region of the neurite is free of the substrate, whereas numerous adhesions in the proximal region cause the neurite to remain firmly fixed. (C) Under constant tension (F_0), the behavior of a Burgers element is dominated by its free dashpot. We treat a neurite under constant tension as a series of dashpots. Attachments to the substrate are represented as friction dashpots (constant η). Tension is constant in the distal region but is dissipated by adhesions in the proximal region.

to recover for several hours in fresh media (9). Cultured cells were maintained at 38°C on the stage in a ringcubator (27). A reference needle and a calibrated needle (calibration constant k, as in (13,22,28,29)) were held in a double-needle holder in a Narishige hydraulic micromanipulator. The needles were brought into the culture dish's microscopic viewing field of a Leica DM IRB inverted microscope and observed with an N Plan L 40×/0.55 corr Ph2 with an adjustable collar infinity/0–2/c objective. Cells were illuminated with a 100-W xenon lamp attenuated 98% with neutral density filters through a Texas Red cube D560/40×, 590DCLP, D630/60m (Chroma, Rockingham, VT) for visualization of MitoTracker Red CMX-Ros.

The calibrated towing needle was previously coated in polylysine (1 mg/ml) and concanavalin A (1 mg/ml). Both needles were brought to the neurite's growth cone and the growth cone was manipulated onto the calibrated towing needle. The manipulator was used to move the needle and exert axial tension on the growth cone (22). Each tow consisted of two phases and within each phase the force was held constant. The resting distance, r, between the two needles was noted before cell attachment. Force measurements were acquired during phase imaging throughout the experiment by measuring the distance, d, between the reference needle and the calibrated needle under experimental tension. The screen-image calibration factor, α, was determined by use of images of a stage micrometer. The applied force at the growth cone (in μdynes) was calculated as $F_0 = \alpha k(d - r)$ (22). Fluorescent images were taken at 2-min intervals by an automated script of the Openlab program (Improvision, Waltham, MA) using a Hamamatsu Orca-ER digital camera CCD, model CA742-95. These images were then converted into TIFFs and analyzed using ImageJ (National Institutes of Health). Images were rotated using an ImageJ plug-in and the StackReg macro was used to align each sequence of images. The images were then cropped, resliced, and z-projected to produce a kymograph. Kymographs were enlarged 2× and brightness and contrast were manipulated to enhance visualization of mitochondria.

Derivation of model

As axons are thought to be viscoelastic structures, we hypothesize that forces generated at the growth cone can stretch the axon and give rise to LVT. Whether this LVT occurs will depend on the relationship between the magnitude of the force generated at the growth cone and the viscoelastic properties of the axon. Even though axons can behave like fluids, if they are exceptionally stiff or if the forces generated at the growth cone are too weak, axonal stretching may not occur and elongation will occur through tip growth.

We consider an axon that experiences a constant force averaged over hours at the growth cone (this tension may be internally or externally generated). For the purpose of a continuous model, we treat the axon as a series of infinitesimally small Burgers elements. If tension is applied for a significant amount of time (>10 min) the axon exhibits a constant growth rate (22). Under these conditions the elastic elements of the cell are at steady state and elongation behaves as force acting on a free dashpot (a dashpot obeys the relationship $force = constant \times velocity$). To analyze bulk transport along the length, we simplify the model and treat the axon, in this state, as a series of dashpots (Fig. 1 C). A series of dashpots under constant tension, without dissipation at each element, has a linear velocity profile which, when additional dashpots are added in series (through elongation), leads to exponential elongation.

As axons stretch, so must the axonal framework. Using the reported value of the Young's modulus of a microtubule of 100 MPa (30), a force of 100 μdynes applied to an individual microtubule will cause ~2% strain. Since a growth-cone-generated force of this magnitude is spread over the cross-sectional area of the axon, the strain on axonal microtubules will be much less. As the stretching of individual polymers is extremely small, significant stretching of the axon most likely occurs by the sliding of cross-linked polymers. The two factors playing the largest role in the velocity profile of an axon under tension are the axon's axial viscosity, g, and the constant of friction, η, which quantifies the interactions between the axon and the substrate. Both of these parameters characterize resistance to flow and have dimensions of viscosity. The axial viscosity is the amount of force needed to distend a unit amount of axon at unit velocity and is determined by the cell's physiological properties. Though the axoplasm is highly heterogeneous, it is the composition of the cytoskeleton that will dictate the axon's response to axial forces. If there is a large number of microtubules, or a high level of cross-linkage between them, then the axon will be resistant to stretching and g will be large (21). Axonal diameter will also affect an axon's ability to be stretched. Intercalated mass addition (axonal thickening) has the effect of adding dashpots, in parallel, to the system (or, equivalently, increasing the dashpot constant). Applied forces are spread over a wider area and effective tension along the length decreases. We define the growth dashpot parameter, G, as quantifying an axon's response to distally applied forces. This parameter is the product of g and the cross-sectional area of the axon, A. If an axon alters its diameter (either thinning due to stretching or thickening by mass addition along the length) but maintains its physiological properties, then G is affected, whereas g is unchanged. Physiological changes alter g and thus G. The coefficient of friction, η, is characterized by the strength and number of adhesions between axon and substrate. These adhesions have been shown to have major effects on both LVT and growth-cone advance (10). η is assumed to be zero where the axon is unattached to the substrate, and increases as adhesions form and strengthen.

Towed axons were observed to be unattached distally and firmly attached to the substrate in the proximal regions (Fig. 1 B). The behavior of the axon in the unattached region can be well described by the three-element model. Our model aims to incorporate the dissipation of forces and describe the velocity profile of docked materials when adhesions are present. We assume that 1), there is uniform dissipation along the length, characterized by the constant η; and 2), during elongation due to towing, the growth dashpot constant G remains fixed on average over a period of days, so that constant applied force implies constant tension. Note that our condition on G is not inconsistent with an axon that changes its diameter; physiological changes can be assumed to balance changes in cell morphology. The phenomenon of strain hardening due to deformation has indeed been observed in various cell types (21). If axons do not exhibit thinning, then we assume that mass addition along the length of the axon, or intercalated mass addition, is responsible for restoring the diameter of axons, which grow by stretching. These assumptions allow for a simple and useful analytic description of the effects of cellular composition and external adhesions on axonal elongation and transport.

Governing equations

The force and velocity profiles of the axons, f and v, are functions of the distance from the cell body, x, and the length of the axon, $L(t)$. A force F_0 applied at the growth cone causes distension at each point along the length. The velocity of material at a position x is given by summing the elongation that is occurring proximal to that point. Viewing the axon as a series of dashpots we find that the change in velocity of elongation, v_x, at each point is given by $v_x(x, L(t)) = f(x, L(t))/G$. The true velocity of material (with respect to the extracellular matrix) at position x is given by integrating v_x from the cell body to x:

$$v[x, L(t)] = \int_0^x v_y[y, L(t)]dy = \int_0^x \frac{f[y, L(t)]}{G}dy.$$

In the discrete case, friction is modeled by dashpots with constant η (Fig. 1 C). The continuous equivalent is the frictional relationship where the change in dissipation at each point is given by $f_{\eta_x}(x, L(t)) = -\eta v(x, L(t))$. The sign is negative, as the most force has been dissipated at the cell body and none has been dissipated at the growth cone. The total amount of force $f_\eta(x, L(t))$ that has been dissipated from F_0 at a point x is found by summing the force dissipation that occurs between x and the growth cone:

$$f_\eta(x, L(t)) = \int_{L(t)}^x f_{\eta_y}(y, L(t)) dy = \int_x^{L(t)} \eta v(y, L(t)) dy$$

$$= \frac{\eta}{G} \int_x^{L(t)} \int_0^y f(z, L(t)) dz dy.$$

The effective force f at a point x is thus the difference between the applied force, F_0, and the dissipation, f_η:

$$f(x, L(t)) = F_0 - \frac{\eta}{G} \int_x^{L(t)} \int_0^y f(z, L(t)) dz dy. \quad (1)$$

This integral equation is equivalent to the differential equation and boundary conditions

$$\begin{cases} f_{xx}(x, L(t)) - \dfrac{\eta}{G} f(x, L(t)) = 0 \\ f(L(t), L(t)) = F_0 \quad f_x(0, L(t)) = 0 \end{cases}. \quad (2)$$

Note that Eq. 2 is in terms of the unknown $L(t)$. The rate of elongation, dL/dt, is assumed to be the velocity of material at the growth cone $v(L(t), L(t))$. Differentiating Eq. 1 with respect to x, we find $f_x(x, L(t)) = \eta/G \int_0^x f(z, L(t)) dz = \eta v(x, L(t))$. Now we can express the change in length of the axon in terms of the force by

$$\begin{cases} \dfrac{dL}{dt} = v(L(t), L(t)) = \dfrac{1}{\eta} f_x(L(t), L(t)) \\ L(0) = L_0 \end{cases}. \quad (3)$$

Force, velocity, and length

Equation 2 is solved first, and the solution for f is then inserted into Eq. 3.

$$f(x, L(t)) = \frac{F_0 \cosh(x(\eta/G)^{1/2})}{\cosh(L(t)(\eta/G)^{1/2})} \quad (4)$$

and

$$L(t) = (G/\eta)^{1/2} \sinh^{-1}\left(\beta \exp\left(\frac{F_0 t}{G}\right)\right), \quad (5)$$

where $\beta = \sinh(L_0(\eta/G)^{1/2})$. Velocity is determined from the force, as before ($v = f_x/\eta$):

$$v(x, L(t)) = \frac{F_0 \sinh(x(\eta/G)^{1/2})}{(\eta G)^{1/2} \cosh(L(t)(\eta/G)^{1/2})}. \quad (6)$$

Nondimensionalization has been performed on the above system. For this discussion, the analysis is clear enough that we retain the dimensional equations.

Data analysis

We tested the predictions of this model by examining the movement of axoplasm in response to tension, as described in Materials and Methods. To fully analyze bulk transport of docked materials, the fluorescent images of each trial were converted into kymographs (9). These useful images were created for each experiment, giving the total profile of movements within each axon over the course of the tow (Fig. 2). Tracing individual mitochondria, average velocities of docked material were calculated over 30-min intervals (Fig. 3). For each tow, there was an observed region where the axon was free of the substrate (distal) and a region where the axon was firmly
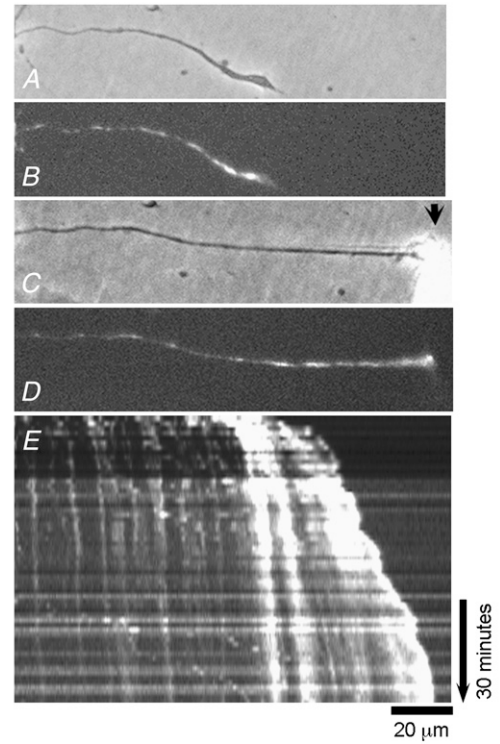

FIGURE 2 Application of force at the growth cone leads to anterograde translocation of docked mitochondria. (A) Axonal morphology at the light level before a tow. The growth cone is toward the righthand side. (B) Mitochondrial distribution before the tow. (C) Axonal morphology at the light level after the tow. The arrow points to the end of the needle at the growth cone. (D) Mitochondrial distribution after the tow. (E) Kymograph illustrating mitochondrial movement during a tow. (F) The graph shows that the velocity of docked mitochondria increases nonlinearly along the axon.

attached (proximal). The distal region, being free of dissipative forces of substrate interaction, was analyzed to extract values of G for the axon. Lines were fitted to this data to calculate the rate of change of the velocity of the mitochondria (Fig. 4 A). Using force measurements from the calibrated needles, a value of G was found by dividing the average force over this interval by the slope of the fitted line.

Once values of G were determined (one value of G/30-min interval) the Origin software package (OriginLab, Northampton, MA) was used with Eq. 6 to fit the best value of η to the data (Fig. 4 B). For this calculation, the velocities of mitochondria proximal to the point of adhesion were used. Empirical values of F_0, L, and G were fixed and a Levenberg-Marquardt algorithm was implemented in the Origin package to find the optimal value of η.

The relationship $G = gA$ was used to calculate the intrinsic axial viscosity for each axon. Phase images of each trial were analyzed using ImageJ to
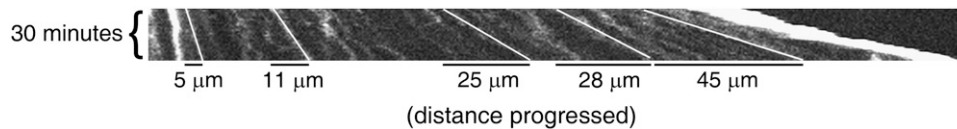
FIGURE 3 Illustration of how velocity data were acquired. Docked mitochondria are observed to translocate anterogradely during a tow. Velocities (in μm/h) of the mitochondria were calculated as the slope of each traced line. Mitochondria near the growth cone move forward at high velocities. whereas mitochondria near the cell body move slowly.

determine the axonal diameter at various times (Fig. 5). For each phase image, the diameter was measured at 25-μm intervals until the growth cone was reached. A line tool was traced orthogonally across the neurite and a plot profile graphed the pixel intensity of the image at each point on the line. It was determined that the best measure of the diameter was the distance between the two steepest points on the intensity curve.

Numerical simulation

To address the issue of thinning along the length of the axon, we ran a MATLAB (The MathWorks, Natick, MA) simulation of an axon growing by stretching, where zero mass addition was assumed and axonal diameter was allowed to vary. The details of the simulation are as follows. The axon is divided into a fixed number of compartments whose length and cross-sectional area are allowed to vary. At each time step, the force is calculated at the distal end of each compartment. This force causes deformation of each compartment and, thus, lengthening. New values for compartment length, area, and growth dashpot parameter, G, are then calculated for the next time step. Though η is constant, we account for the adhesive effect of increased compartment length. Using parameter values for g and η determined as above, axons were allowed to grow until the cross-sectional area at any point along the length decreased below 0.05 μm^2 (or, equivalently, until the diameter at any point decreased below 0.25 μm). This basic simulation does not take into account protein degradation or axonal transport of existing materials that may occur to maintain a uniform diameter. The code is available online as Supplementary Material.

RESULTS

Consistency

We verify that the model equations are consistent with the physical nature of the problem. Letting the parameters vary, we examine the effects on Eq. 6. The following calculations are limit computations using L'Hôpital's rule. It is important to remember, here, that η characterizes adhesions along the length of the axon and not at the growth cone. As adhesions at

the growth cone are necessary for tension generation, our model would predict that those adhesions increase rates of elongation.

The removal of adhesive connections along the length corresponds to η going to zero. In this case, forces generated at the growth cone are not dissipated through the substrate and we should expect a linear velocity profile, as that is the behavior of a series of dashpots under tension. Indeed, it can be shown as $\eta \rightarrow 0$ that $v(x, L(t); \eta) \rightarrow F_0 x/G$, which is the solution of the dissipation-free problem.

In the presence of strong adhesions, forces are dissipated quickly and transport is hindered. Large values of η describe this phenomenon. For a fixed force, if η is too large, then the effective tension along the length of the axon is too low to facilitate transport. As the strength of the adhesions increases, $\eta \rightarrow \infty$ and $v(x, L(t); \eta) \rightarrow 0$ for all x.

If G is relatively large, then the axon will be resistant to stretching at normal forces. This will occur when an axon has a large diameter or if there is a great deal of microtubule cross-linkage. A direct calculation shows $v(x, L(t); G) \rightarrow 0$ for all x, as $G \rightarrow \infty$.

Last, we consider the case where $G \rightarrow 0$. If G is very small at a point x, then either the diameter of the axon is close to zero at that point ($A \approx 0$) or there is little cellular structure at x holding the axon together ($g \approx 0$). In either case, the applied tension causes rapid deformation at x, but forces are quickly absorbed into the substrate and are not proximally propagated. The tension gradient causes a sharp jump in the velocity of materials at x, making the axon prone to "rupturing". This behavior is captured by Eq. 6 as

$$\lim_{G \rightarrow 0} v(x, L(t); G) = \begin{cases} 0 & 0 \leq x < L(t) \\ \infty & x = L(t) \end{cases}.$$
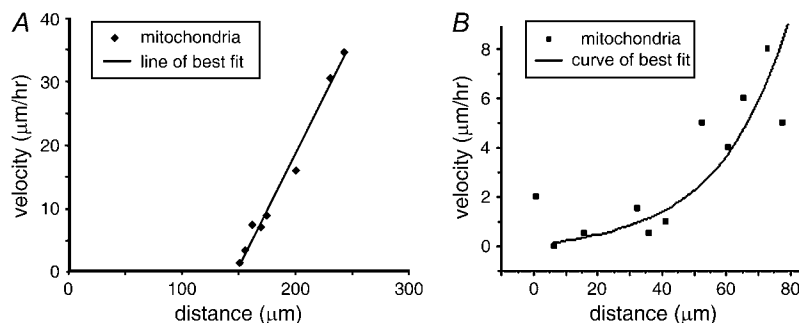

FIGURE 4 Determination of axonal viscosity (G) and adhesiveness (η). During towing, the distal axon was lifted free from attachments to the substrate. (A) Velocities were measured (one measurement/mitochondria/30 min) for mitochondria distal to the terminal point of adhesion between axon and substrate (for this axon, at 150 μm). The slope, m, of the line of best fit and the force, F_0, are related to G by $G = F_0/m$. (B) Velocity profile of mitochondria proximal to the terminal point of adhesion (at 80 μm for this trial). Force dissipation leads to a nonlinear velocity profile. The data was fitted to Eq. 6 with an optimal value of η found using the Origin software package.
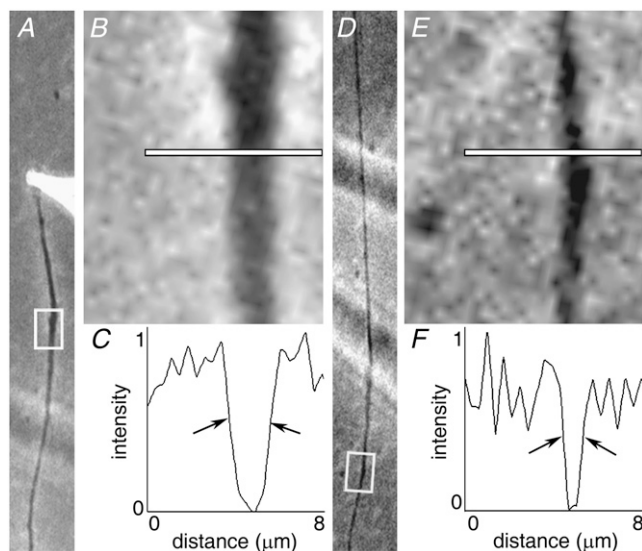
FIGURE 5 Illustration of the measurement of axonal diameter. For each phase image (*A* and *D*), the diameters of the axons were measured using ImageJ (one measurement/25 μm). A line orthogonal to the axon was drawn (*B* and *E*) and a plot profile gives the pixel intensity at each point along the line (*C* and *F*). Arrowheads in *C* and *F* denote the two steepest points on the relevant portion of the curve. Visible differences in axonal diameter (*A* and *D*) are reflected in *C* and *F*.

Parameter values

Average values for G, g, and η were found as described in Materials and Methods. The average value of G was found to be $\bar{G} = 3.9 \times 10^7 \pm 3.0 \times 10^7$ g μm h^{-1} (mean $\pm$ SD, $n = 31$). The intrinsic value g for each axon at each 30-min period was found by dividing G by the average cross-sectional area of the axon distal to the initial point of adhesion. We found this value to have an average of $\bar{g} = 1.3 \times 10^7 \pm 8.5 \times 10^6$ g μm^{-1} h^{-1} (mean $\pm$ SD, $n = 31$), which is equivalent to $3.6 \times 10^6 \pm 2.4 \times 10^6$ Pa·s (1 Pa·s = 3.6 g μm^{-1} h^{-1}). The average η value was $\bar{\eta} = 9.6 \times 10^3 \pm 7.5 \times 10^3$ Pa·s (mean $\pm$ SD, $n = 28$). In three cases, there was an insufficient number of mitochondria proximal to the initial point of adhesion to be able to fit a significant value of η.

Model predictions

As a test of the model, we plotted Eq. 6 with the calculated average parameters and a force of 200 μdynes against data from neurons growing naturally on laminin/polyornithine substrates. Using velocity measurements from 13 arbors of six growing axons ($N = 563$), we observed significant LVT of the distal axon and found a strong correlation between our model and the actual level of stretching (Fig. 6 *A*). An interesting observation in this process was that the majority of docked mitochondria in the proximal regions, where growth
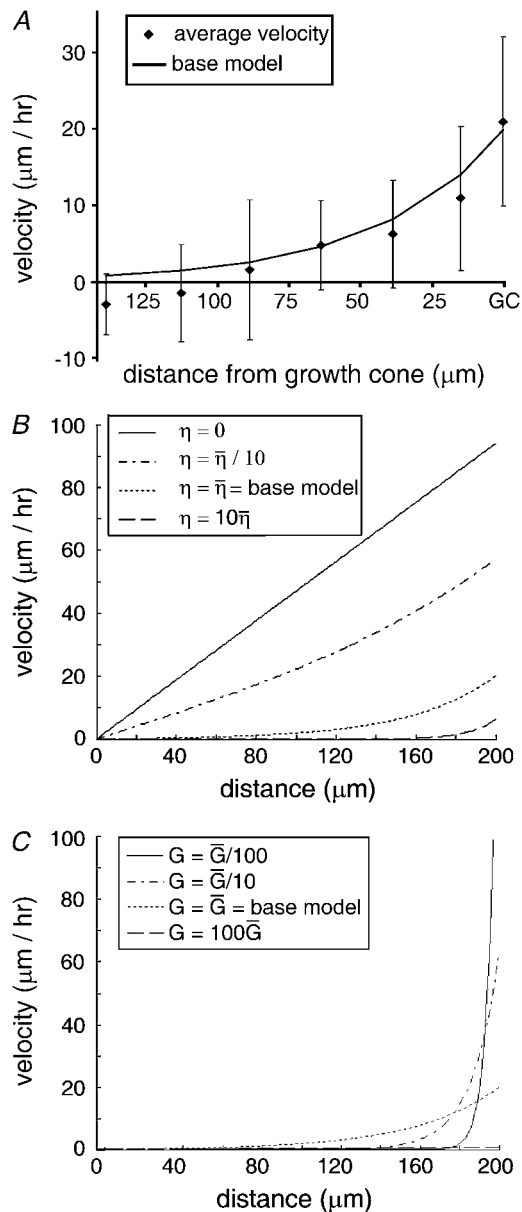

FIGURE 6 Whether axonal stretching occurs along the length or only at the tip depends on the values of G and η (*A*). Comparison of the base model with data from axons growing naturally on laminin/polyornithine substrates. Velocities of docked mitochondria from arbors of six different neurons were recorded ($N = 563$). Average velocities were then calculated at the growth cone and for each 25-μm segment proximal. Comparison of the average velocities with the base model yielded an R^2 value of 0.81. (*B* and *C*) Model sensitivity to parameters. (*B*) For large values of η (strong adhesions), forces are dissipated quickly and very little bulk transport is observed. When adhesions are absent ($\eta = 0$), the force is not dissipated and the velocity profile is linear (like a series of dashpots). $L = 200$ μm, $F_0 = 200$ μdynes, $G = \bar{G}$. (*C*) Large G values cause low effective friction (η/G) and result in low velocity at the growth cone with little force dissipation along the length. Small G values lead to high velocities near the source of tension. Because effective friction is high, forces are quickly dissipated and velocity of materials goes to zero a short distance away from the growth cone. This behavior leads to rapid elongation, but possible rupturing of the axon. $L = 200$ μm, $F_0 = 200$ μdynes, $\eta = \bar{\eta}$.

cone generated forces have little effect, moved in the retrograde direction.

Having analyzed the behavior of the velocity profile for extreme values of G and η, we focus on how the velocity profile changes with the parameters. Plots of Eq. 6 for varying magnitudes of η and G are displayed in Fig. 6, B and C. As the effect of the neurite/substrate interactions (η) increases, less of the neurite experiences bulk transport, with the most transport occurring near the growth cone. If adhesive forces are not present, then transport behaves as a system of dashpots, with the velocity of docked material increasing linearly. Variations in the growth dashpot parameter, G, cause different types of changes. If G is relatively large, the neurite is too stiff, and realistic forces are insufficient to produce significant bulk transport or elongation (Fig. 6 C, *dashed line*). As the neurite becomes more fluid (G decreases) both bulk transport and elongation are observed. Notice that, in the presence of adhesions, transport is still minimal in the proximal axon. Decreasing G further, transport occurs only in the distal axon with a steep gradient (Fig. 6 C, *solid line*). An extremely small value of G represents an axon that is too fluid to withstand tension. This neurite will see a sharp change from zero velocity of materials in the majority of the axon to extreme stretching near the growth cone. The neurite offers little resistance to tension, but the tension dissipates immediately, possibly leading to rupture at the point where the tension is applied. An observed axonal rupture is explained by this model as G being locally too small to handle the forces in that region.

In the towed growth experiments, where the velocity of axonal elongation exceeds the normal rate of elongation, axons thinned. In contrast, in the naturally growing axons, dramatic thinning was not observed. This suggests that there is some rate of mass addition that occurs along the length of the axon that normally prevents axonal thinning, but that when the normal growth rate is exceeded there is initially a thinning of the axon. Our simulation of a growing axon without mass addition is consistent with this observation (Fig. 7). The force generated at the growth cone (200 μdynes) causes lengthening of the axon and thinning. Force dissipation due to adhesions restricts thinning to the distal region, and, in a short amount of time, the diameter becomes extremely small at the growth cone. Comparison of our simulation with the profiles of naturally growing axons implies that mass addition counteracts stretch-induced thinning.

The model predicts that for a given set of parameters (F_0, G, and $\eta > 0$) a growing axon achieves a maximum velocity of axonal elongation (Fig. 8). Further, it shows that there is a characteristic velocity profile that advances with the growth cone and is nonzero for some fixed length from the growth cone $\bar{L}$. For very short axons, forces generated at the growth cone are not fully dispersed along the length, and the velocity profile is nearly linear. As the axon elongates, the actual velocity of the materials near the growth cone increases to its maximum value $v_{\max} = F_0/(G\eta)^{1/2}$ and the velocity profile
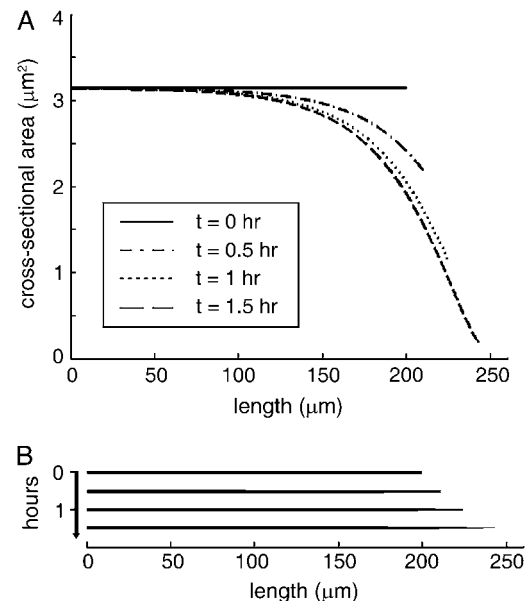
FIGURE 7 Without mass addition, axons thin when stretched. To examine the necessity of intercalated mass addition, Euler's implementation was employed in which cross-sectional area was allowed to vary while the axon lengthened. The growth dashpot parameter, G, and the constant of friction, η, were initially set at physiological levels ($g = \bar{g}$, $A = \pi \ \mu\text{m}^2$, $\eta = \bar{\eta}$). During lengthening, G varied with the cross-sectional area while η was held constant. Here, we simulated an axon that was initially 200 μm long, with a uniform axonal diameter of 2 μm, and a constant force of 200 μdynes applied at the growth cone. The simulations ran until the cross-sectional area became smaller than 0.05 μm^2 at any point. (*A*) The profile of the cross-sectional area over the first 1.5 h of growth demonstrates that the force gradient due to cell-substrate adhesions leads to nonuniform thinning in the distal region. (*B*) A scale representation of the axon over the first 1.5 h of growth strongly suggests that intercalated mass addition occurs to prevent thinning.

attains its exponential shape. Once the axon is long enough ($L \geq \bar{L}$) that force dissipation causes the velocity to reach zero before the growth cone, the velocity curve behaves, over time, as if it were shifting to the right.

DISCUSSION

How axons elongate has been a central debate in neurobiology for decades. Tip growth is generally accepted as the method (1,31), but stretching has been observed along the axons of *Xenopus* neurons and in the distal axon of chicken sensory neurons (9,19,20). It is well agreed that growth cones generate tension (32) and cells are viscoelastic materials (21) that adhere to substrates (10). Thus, it seems reasonable to conclude that axons stretch in response to forces. To test this, we use direct observation of the movements of docked mitochondria and physical manipulation of the neurons via axonal towing to test whether axons stretch in response to force application at the growth cone and to determine the normal parameters for the viscosity of the axon and the level of adhesion to the substrate. We then mathematically model
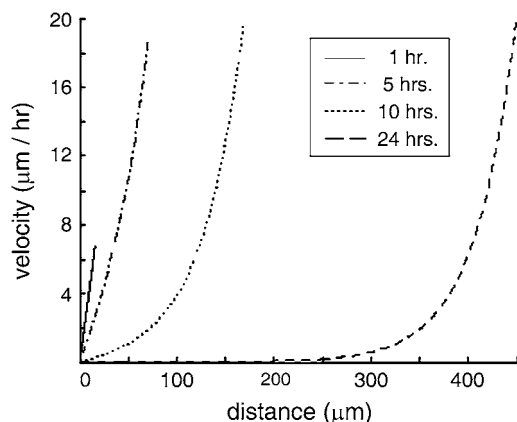
FIGURE 8 Nascent axons elongate slowly. A simulation of an initially short axon ($L_0 = 10$ μm) under tension shows the velocity profile of an elongating axon. Transport is present along the length when the axon is short and the elongation rate is low. As the axon grows, the velocity of elongation increases until the length of the region where transport is observed reaches a maximum (here, ~100 μm). The velocity profile then translocates, with an increasing lagging zone in the proximal axon where no transport is observed. $F_0 = 200$ μdynes, $G = \bar{G}$, $\eta = \bar{\eta}$.

the axon as a viscoelastic fluid, based on the work of Dennerll et al., which suggests that tip growth occurs when the forces generated at the growth cone are weak, the adhesions along the axon are strong, or the viscosity of the axon is high.

Although it is well accepted that force application at the growth cone leads to axonal elongation (11,13), whether it leads to stretching of the axon has not been addressed. Anterograde LVT of the distal cytoskeleton, as previously documented (9,10,18–20), was present in our control experiments (Fig. 6 A). To test the effects of external force application, we monitored the movement of docked mitochondria along the axon while towing. We observed that mitochondria along the axon translocated in an anterograde manner (Fig. 2 E) and with a velocity profile that was strongly nonlinear (Fig. 2 F). The velocity of movement of the docked mitochondria was directly linked to the rate of towing. When axons were towed at a rate of 50 μm h^{-1} the velocity of mitochondrial movement next to the growth cone was ~40 μm h^{-1} (Fig. 2 F), and when towing occurred at 100 μm h^{-1}, the velocity of movement next to the growth cone was ~90 μm h^{-1}. Together, these data provide the first direct evidence that the external application of forces to the growth cone leads to stretching of the axon.

The key test for our model was to examine the velocity profile in regions of the axon that were unattached (Fig. 4 A) and attached (Fig. 4 B) to the substrate. If our model is correct, then the velocity profile would be linear in the unattached regions and nonlinear in the attached regions. We found that the data support a model where adhesions along the axon dissipate forces exerted at the growth cone. By estimating the cross-sectional area of the axon (Fig. 5), we calculated the true viscosity (g) to be $3.6 \times 10^6 \pm 2.4 \times 10^6$ Pa·s on average. This measurement is comparable to obser-

vations made in fibroblasts, which suggest that the cytoplasmic viscosity is between 10^2 and 10^6 Pa·s (33). The elevated value reported here is not surprising, given that the axial viscosity of a neurite is a function of deformation-resistant features such as cross-linked cytoskeletal elements within the axon (21,34,35). An important control was to compare the velocity profile of docked mitochondria along the axon during normal axonal elongation with the velocity profile prediction based on our direct estimates of G, η, and the magnitude of force at the growth cone. That our model fits well with the data (Fig. 6 A) illustrates its relevance and predictive power.

The strength of cellular adhesions has previously been measured by means of centrifugation (36) and fluid flow (37) or by the amount of force required to pry a cell from the substrate (28). Although those techniques are useful for determining relative adhesiveness, the results are difficult to apply to other systems, because they are in indirect units (e.g., the fraction of adherent cells after centrifugation and the duration of blasting through a pipette required to detach a cell) or are a complex function of the applied force, viscoelastic properties of the cell, and adhesion. Our description is unique in that it is the first direct estimation of the level of adhesion of an axon to a substrate. Based on our estimation of the level of cellular adhesion to the substrate ($\eta = 9.6 \times 10^3 \pm 7.5 \times 10^3$ Pa·s), we can predict the traction force an axon exerts on the substrate versus the distance from the growth cone. For example, given an endogenous force of 2 nN in chicken dorsal root ganglion growth cones, and an apparent axonal viscosity of 1.1×10^7 Pa·s, we predict that a 1-μm region of axon 10 μm from the growth cone will exert 26 pN of traction force. In situations where axons are elongating by tip growth, we predict that traction force due to adhesions will drop off very rapidly away from the growth cone and will be zero along the axon. In contrast, traction forces will decline gradually toward the cell body in cases where axons are elongating by stretching (i.e., in dorsal root ganglion neurons grown on laminin/polyornithine). Further experiments monitoring axonal elongation using plastic pads mounted on cantilevers (38) or micropatterned elastomer substrates (39) will allow our model and predictions to be tested directly.

A key finding of Chang et al. (10) was that the substrate on which a neuron was grown determined whether the axons grew by stretching or by tip growth. Furthermore, axons that stretched grew more quickly than axons that were attached to the substrate. Our model behaves in a similar fashion (Fig. 6, B and C). A possible insight into the problem of axonal elongation suggested by our model is that axons typically extend by stretching of the distal axon, but when the adhesions along the axon are strong, stretching only occurs at the tip. Although tip growth and axonal stretching appear to be qualitatively different, our model suggests that tip growth may just be a special case where stretching is restricted to the growth cone.

The tip growth model predicts that axonal elongation occurs by the addition of new mass at the growth cone. Depending on the school of thought, this occurs either through microtubule polymerization at the growth cone (1,31) or the addition of new microtubules by stop-and-go transport (40). In both cases, increasing the amount of microtubule polymer has the predicted effect of increasing the rate of axonal elongation. For values of G and η that are reasonably greater than zero, our model predicts that the elongation rate of an axon attached to the substrate is proportional to $F_0/(G\eta)^{1/2}$. Thus, an increase in G due to polymerization leads to a decline in the velocity of elongation. In other words, the rate of axonal elongation is sensitive to the viscosity of the axon: the higher the viscosity, the slower the rate of axonal elongation. This suggests an explanation to the counterintuitive observation that an increase in microtubule polymerization through the application of the drug taxol slows the rate of axonal elongation (17,41). Our model predicts that an increase in microtubule mass along the length will slow the rate of axonal elongation by increasing the viscosity of the axon (Fig. 6 C). In the case of taxol application, it suggests that the axons elongate more slowly because tubulin is converted to microtubules along the length and the viscosity (G) of the axon increases.

A related issue is the question of why axons are thin during elongation and then increase in diameter after synapse formation (42). Our model suggests that the apparent viscosity (G) of the axon is a function of axonal diameter, and that thin axons will thus grow more quickly given a level of tension at the growth cone. The relationship between axonal diameter and rate of growth may also explain why thin neurites of Aplysia neurons (2–6 μm in diameter), but not the main axonal trunk (20–50 μm) advance in tissue culture (43). How axonal elongation varies with axonal viscosity and diameter has not been systematically addressed experimentally and will be an interesting avenue for future research.

The observation that rapidly advancing growth cones are small and growth cones that pause enlarge (44) further suggests that mass addition does not control the rate of axonal lengthening. In the context of our model, for a given rate of mass addition there exists a critical level of stretching that would result in no change in diameter. The aforementioned observations could be interpreted such that rapidly advancing growth cones are small because they undergo a supercritical degree of stretching, and paused and slowly advancing growth cones enlarge because the level of stretching is subcritical. In this context, our assumption that G is constant during elongation is equivalent to saying that the rate of mass addition increases with the rate of lengthening.

Where mass addition occurs during axonal elongation is a long-standing problem (4). A simulation of an axon growing by stretching revealed that, without mass addition, thinning of the distal region to a very small diameter ($<$250 nm) occurs in a matter of hours (Fig. 7). Because axons grown naturally on laminin are not observed to thin significantly, this suggests that mass addition is occurring along the distal axon.

Any model of axonal elongation must account for the observation that axons tend to lengthen at some average rate that does not seem to significantly vary with the length of the axon (45). The inclusion of adhesions along the axon in our model produces this behavior, preventing unbounded elongation rates (Fig. 8). Presuming that growth cones generate similar amounts of force in short and long axons, the region of axonal stretching and force dissipation is similar regardless of the length of the axon and advances with the growth cone. This creates a region of axonal stretching in the distal axon, yet a stationary cytoskeletal framework in the proximal axon.

There are several potential shortcomings of our model. The first is that we place mass addition as a dependent variable instead of an independent variable that controls the rate of axonal lengthening. Although we based this on our interpretation of the available experimental data, as outlined in the Introduction, further studies are required to definitively demonstrate the site of mass addition along the axon. The second limitation is that our model is one-dimensional and does not address the two- or three-dimensional problem of axonal guidance. We think this is an exciting question (25), but deeper knowledge of the interactions between the axonal shaft and substrate will be required, in particular, to determine whether adhesions are discrete or continuous. The third potential limitation is that we treat the axon as a stiff viscoelastic fluid and ignore elastic behaviors. We agree that an understanding of those processes is important, especially in the context of the problem of axonal guidance in short timescales up to several hours. The final limitation is that we do not consider the dynamic aspects of axonal elongation. For example, it is well accepted that sensory neurons do not thin over extended periods of time during elongation on glass coverslips coated with laminin (5), in vivo during lengthening forced by bone elongation (16), or in vitro during towed growth at rates as high as 8 mm/day (14). Thus, in our model, we hold axonal diameter, G, and η to be constant for the steady-state solution. Yet, as is seen in Fig. 5, A and D, which is a representative example, axonal diameter appears to decrease during lengthening caused by towing. We believe that this thinning might occur because the rate of mass addition does not rapidly adjust to changes in the rate of axonal lengthening (14). These results suggest that future models that incorporate dynamic aspects (such as changes in the velocity of elongation) may also need to include changes in axonal diameter, g, and in mass addition as functions of the rate of axonal lengthening.

CONCLUSION

As axons are viscoelastic, forces may play a role in elongation and bulk transport of materials. We have proposed a model that suggests that the extent of neuronal lengthening is dictated by tension, the physical viscoelastic properties of the

axon, and the axon's surrounding environment. The model suggests that tip growth may be a special case where axonal stretching is restricted to the growth cone because the level of adhesions along the axon are very high, the viscosity or thickness of the axon is large, or force generation in the growth cone is weak.

SUPPLEMENTARY MATERIAL

To view all of the supplemental files associated with this article, visit www.biophysj.org.

REFERENCES

1. Dent, E. W., and F. B. Gertler. 2003. Cytoskeletal dynamics and transport in growth cone motility and axon guidance. *Neuron.* 40: 209–227.

2. Brown, A. 2003. Axonal transport of membranous and nonmembranous cargoes: a unified perspective. *J. Cell Biol.* 160:817–821.

3. Hirokawa, N., S. Terada, T. Funakoshi, and S. Takeda. 1997. Slow axonal transport: the subunit transport model. *Trends Cell Biol.* 7: 384–388.

4. Bray, D. 1970. Surface movements during the growth of single explanted neurons. *Proc. Natl. Acad. Sci. USA.* 65:905–910.

5. Bray, D. 1973. Branching patterns of individual sympathetic neurons in culture. *J. Cell Biol.* 56:702–712.

6. Lim, S. S., K. J. Edson, P. C. Letourneau, and G. G. Borisy. 1990. A test of microtubule translocation during neurite elongation. *J. Cell Biol.* 111:123–130.

7. Okabe, S., and N. Hirokawa. 1990. Turnover of fluorescently labelled tubulin and actin in the axon. *Nature.* 343:479–482.

8. Chang, S., T. M. Svitkina, G. G. Borisy, and S. V. Popov. 1999. Speckle microscopic evaluation of microtubule transport in growing nerve processes. *Nat. Cell Biol.* 1:399–403.

9. Miller, K. E., and M. P. Sheetz. 2006. Direct evidence for coherent low velocity axonal transport of mitochondria. *J. Cell Biol.* 173:373–381.

10. Chang, S., V. I. Rodionov, G. G. Borisy, and S. V. Popov. 1998. Transport and turnover of microtubules in frog neurons depend on the pattern of axonal growth. *J. Neurosci.* 18:821–829.

11. Bray, D. 1984. Axonal growth in response to experimentally applied mechanical tension. *Dev. Biol.* 102:379–389.

12. Lamoureux, P., G. Ruthel, R. E. Buxbaum, and S. R. Heidemann. 2002. Mechanical tension can specify axonal fate in hippocampal neurons. *J. Cell Biol.* 159:499–508.

13. Zheng, J., P. Lamoureux, V. Santiago, T. Dennerll, R. E. Buxbaum, and S. R. Heidemann. 1991. Tensile regulation of axonal elongation and initiation. *J. Neurosci.* 11:1117–1125.

14. Pfister, B. J., A. Iwata, D. F. Meaney, and D. H. Smith. 2004. Extreme stretch growth of integrated axons. *J. Neurosci.* 24:7978–7983.

15. Pfister, B. J., D. P. Bonislawski, D. H. Smith, and A. S. Cohen. 2006. Stretch-grown axons retain the ability to transmit active electrical signals. *FEBS Lett.* 580:3525–3531.

16. Abe, I., N. Ochiai, H. Ichimura, A. Tsujino, J. Sun, and Y. Hara. 2004. Internodes can nearly double in length with gradual elongation of the adult rat sciatic nerve. *J. Orthop. Res.* 22:571–577.

17. Letourneau, P. C., and A. H. Ressler. 1984. Inhibition of neurite initiation and growth by taxol. *J. Cell Biol.* 98:1355–1362.

18. Okabe, S., and N. Hirokawa. 1993. Do photobleached fluorescent microtubules move? Re-evaluation of fluorescence laser photobleaching both in vitro and in growing *Xenopus* axon. *J. Cell Biol.* 120:1177–1186.

19. Okabe, S., and N. Hirokawa. 1992. Differential behavior of photo-activated microtubules in growing axons of mouse and frog neurons. *J. Cell Biol.* 117:105–120.

20. Reinsch, S. S., T. J. Mitchison, and M. Kirschner. 1991. Microtubule polymer assembly and transport during axonal elongation. *J. Cell Biol.* 115:365–379.

21. Heidemann, S. R., and D. Wirtz. 2004. Towards a regional approach to cell mechanics. *Trends Cell Biol.* 14:160–166.

22. Dennerll, T. J., P. Lamoureux, R. E. Buxbaum, and S. R. Heidemann. 1989. The cytomechanics of axonal elongation and retraction. *J. Cell Biol.* 109:3073–3083.

23. Sato, M., T. Z. Wong, D. T. Brown, and R. D. Allen. 1984. Rheological properties of living cytoplasm: a preliminary investigation of squid axoplasm (*Loligo pealei*). *Cell Motil.* 4:7–23.

24. Aeschlimann, M. 2000. Biophysical models of axonal pathfinding. PhD thesis. Faculty of Science, University of Lausanne, Lausanne, Switzerland.

25. Aeschlimann, M., and L. Tettoni. 2001. Biophysical model of axonal pathfinding. *Neurocomputing.* 38:87–92.

26. Sinclair, G. I., P. W. Baas, and S. R. Heidemann. 1988. Role of microtubules in the cytoplasmic compartmentation of neurons. II. Endocytosis in the growth cone and neurite shaft. *Brain Res.* 450: 60–68.

27. Heidemann, S. R., P. Lamoureux, K. Ngo, M. Reynolds, and R. E. Buxbaum. 2003. Open-dish incubator for live cell imaging with an inverted microscope. *Biotechniques.* 35:708–714, 716.

28. Zheng, J., R. E. Buxbaum, and S. R. Heidemann. 1994. Measurements of growth cone adhesion to culture surfaces by micromanipulation. *J. Cell Biol.* 127:2049–2060.

29. Zheng, J., R. E. Buxbaum, and S. R. Heidemann. 1993. Investigation of microtubule assembly and organization accompanying tension-induced neurite initiation. *J. Cell Sci.* 104:1239–1250.

30. Kis, A., S. Kasas, B. Babic, A. J. Kulik, W. Benoit, G. A. Briggs, C. Schonenberger, S. Catsicas, and L. Forro. 2002. Nanomechanics of microtubules. *Phys. Rev. Lett.* 89:248101.

31. Graham, B. P., and A. van Ooyen. 2006. Mathematical modelling and numerical simulation of the morphological development of neurons. *BMC Neurosci.* 7(Suppl 1: S9):1–12.

32. Lamoureux, P., R. E. Buxbaum, and S. R. Heidemann. 1989. Direct evidence that growth cones pull. *Nature.* 340:159–162.

33. Yamada, S., D. Wirtz, and S. C. Kuo. 2000. Mechanics of living cells measured by laser tracking microrheology. *Biophys. J.* 78:1736–1747.

34. Hirokawa, N. 1982. Cross-linker system between neurofilaments, microtubules, and membranous organelles in frog axons revealed by the quick-freeze, deep-etching method. *J. Cell Biol.* 94:129–142.

35. Schnapp, B. J., and T. S. Reese. 1982. Cytoplasmic structure in rapid-frozen axons. *J. Cell Biol.* 94:667–669.

36. Maheshwari, G., G. Brown, D. A. Lauffenburger, A. Wells, and L. G. Griffith. 2000. Cell adhesion and motility depend on nanoscale RGD clustering. *J. Cell Sci.* 113:1677–1686.

37. Lemmon, V., S. M. Burden, H. R. Payne, G. J. Elmslie, and M. L. Hlavin. 1992. Neurite growth on different substrates: permissive versus instructive influences and the role of adhesive strength. *J. Neurosci.* 12:818–826.

38. Galbraith, C. G., and M. P. Sheetz. 1997. A micromachined device provides a new bend on fibroblast traction forces. *Proc. Natl. Acad. Sci. USA.* 94:9114–9118.

39. Cesa, C. M., N. Kirchgessner, D. Mayer, U. S. Schwarz, B. Hoffmann, and R. Merkel. 2007. Micropatterned silicone elastomer substrates for

high resolution analysis of cellular force patterns. *Rev. Sci. Instrum.* 78:034301.

40. Brown, A. 2000. Slow axonal transport: stop and go traffic in the axon. *Nat. Rev. Mol. Cell Biol.* 1:153–156.

41. Bamburg, J. R., D. Bray, and K. Chapman. 1986. Assembly of microtubules at the tip of growing axons. *Nature.* 321:788–790.

42. Sharma, A. K., S. Bajada, and P. K. Thomas. 1980. Age changes in the tibial and plantar nerves of the rat. *J. Anat.* 130:417–428.

43. Lovell, P., and L. L. Moroz. 2006. The largest cone growth cones in the animal kingdom: an illustrated guide to the dynamics of Aplysia neuronal growth in cell culture *Integr. Comp. Biol.* 46:847–870.

44. Godement, P., L. C. Wang, and C. A. Mason. 1994. Retinal axon divergence in the optic chiasm: dynamics of growth cone behavior at the midline. *J. Neurosci.* 14:7024–7039.

45. Dotti, C. G., C. A. Sullivan, and G. A. Banker. 1988. The establishment of polarity by hippocampal neurons in culture. *J. Neurosci.* 8:1454–1468.